Progress In Electromagnetics Research, PIER 18, 229–244, 1998

NUMERICAL ANALYSIS OF AN APERTURE COUPLED MICROSTRIP PATCH ANTENNA USING MIXED POTENTIAL INTEGRAL EQUATIONS AND COMPLEX IMAGES

D. Yau and N. V. Shuley

Department of Electrical and Computer Engineering
The University of Queensland
Brisbane, Queensland 4072
Australia

1. INTRODUCTION

Much attention has been focussed on the aperture coupled microstrip antenna since its introduction by Pozar [1]. So far, moment method techniques based on the spectral domain approach [2, 3] have been used to deal with the problem. Although these methods generate accurate results, the enormous computational effort required renders them impractical in an actual design environment. In this paper, a mixed potential integral equation (MPIE) approach is developed to analyze the aperture coupled microstrip patch antenna. The method is basically

an extension of [4] to an aperture coupled geometry. The problem is formulated as three coupled integral equations in the spatial domain as opposed to the electric field integral equations in [2]. In order to avoid the formidable numerical task of evaluating the Sommerfeld integrals, closed-form Green's functions [5,6] are employed. The result is a great increase in the overall computation speed while the comprehensiveness of the analysis is maintained.

In [5–7], the closed-form Green's functions for the potentials of an horizontal electric dipole (HED) are derived. Using the same techniques, the closed-form expressions are similarly derived for the potentials of an horizontal electric dipole (HMD) and the associated coupled fields.

2. FORMULATION

The geometry (Fig. 1) is essentially similar to that of [2] except in our formulation the length of feedline is finite. The space above and below the ground plane ($z = 0$) which are the microstrip structure for the radiating antenna and the feedline are denoted as region 1 and 2 respectively. The thickness of the substrate in these respective regions are denoted as h_1 and h_2 . The excitation current and induced current on the feedline are denoted $\mathbf{J}_e$ and $\mathbf{J}_f$; $\mathbf{J}_p$ is the induced current on the patch. Using the equivalence principle, the x-directed E field in aperture can be short circuited and replaced by magnetic surface currents $\mathbf{M}_{ap}$ just above and below the ground plane. If the aperture and feedline have their width much smaller than the operating wavelength, then we can assume the currents flowing on them are only directed along their lengths. To maintain the continuity of tangential electric field through the aperture, we have $\mathbf{M}_{ap}^{(1)} = -\mathbf{M}_{ap}^{(2)} = -\mathbf{M}_{ap} = -\hat{y}\mathbf{M}_{ap}$.

The total fields in each region can be written as the sum of the scattered and excitation fields due to the corresponding potentials:

$$\mathbf{E}_{tot}^{(1)} = \mathbf{E}_A^{(1)}(\mathbf{J}_p) + \mathbf{E}_F^{(1)}(\mathbf{M}_{ap}) \tag{1}$$

$$\mathbf{H}_{tot}^{(1)} = \mathbf{H}_A^{(1)}(\mathbf{J}_p) + \mathbf{H}_F^{(1)}(\mathbf{M}_{ap}) \tag{2}$$

$$\mathbf{E}_{tot}^{(2)} = \mathbf{E}_A^{(2)}(\mathbf{J}_f) + \mathbf{E}_F^{(2)}(\mathbf{M}_{ap}) + \mathbf{E}_A^{e(2)}(J_e) \tag{3}$$

$$\mathbf{H}_{tot}^{(2)} = \mathbf{H}_A^{(2)}(\mathbf{J}_f) + \mathbf{H}_F^{(2)}(\mathbf{M}_{ap}) \tag{4}$$

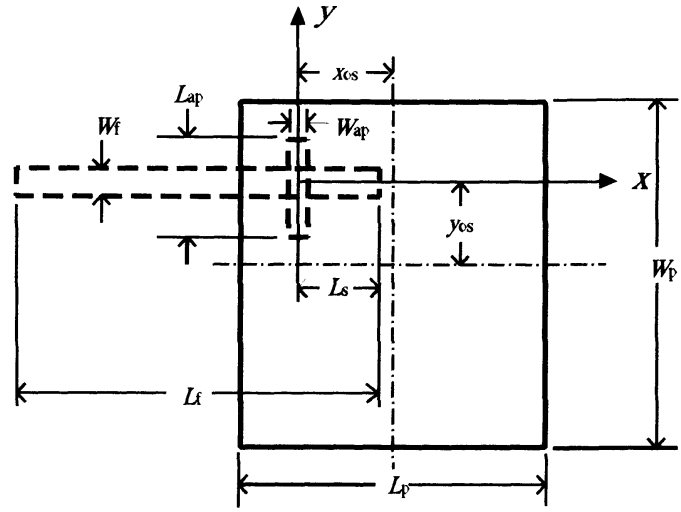

(a)

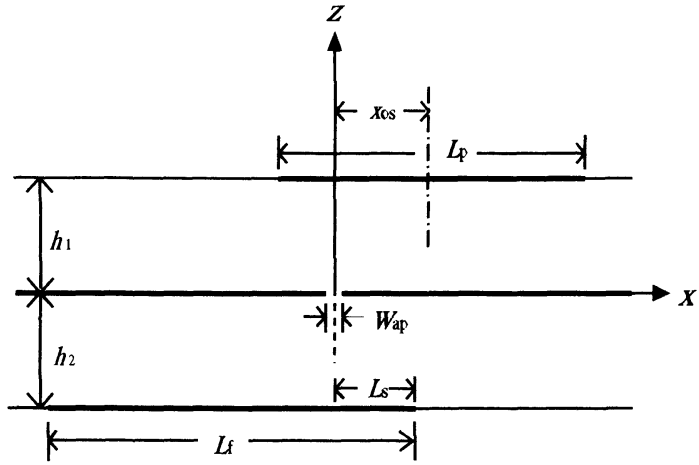

(b)

Figure 1. Geometry of aperture coupled patch antenna. (a) Top view (b) Side view.

where $\mathbf{E}_A$, $\mathbf{H}_A$, $\mathbf{E}_F$, and $\mathbf{H}_F$ (the superscript denotes the region considered) are the fields due the corresponding potentials in each region; $\mathbf{E}^e$ is the excitation electric field in region 2. These are written as

$$\mathbf{E}_A = -j\omega\mathbf{A} - \nabla V \tag{5}$$
$$\mathbf{E}_F = -(1/\epsilon)\nabla \times \mathbf{F} \tag{6}$$
$$\mathbf{H}_A = (1/\mu_0)\nabla \times \mathbf{A} \tag{7}$$
$$\mathbf{H}_F = -j\omega\mathbf{F} - \nabla V_m \tag{8}$$

where $\mathbf{A}$ is the magnetic vector potential, V is the electric scalar potential, $\mathbf{F}$ is the electric vector potential, and V_m is the magnetic scalar potential.

2.1 Green's Functions

The vector and scalar potentials are in turn expressed as convolution integrals of the induced current and charge distributions with the corresponding Green's function:

$$\mathbf{A}(\mathbf{r}|\mathbf{r}') = \int_{S_0} \overline{\overline{\mathbf{G}}}_A(\mathbf{r}|\mathbf{r}') \cdot \mathbf{J}(\mathbf{r}')dS' \tag{9}$$
$$\mathbf{V}(\mathbf{r}|\mathbf{r}') = \int_{S_0} G_v(\mathbf{r}|\mathbf{r}')q(\mathbf{r}')dS' \tag{10}$$
$$\mathbf{F}(\mathbf{r}|\mathbf{r}') = \int_{S_0} \overline{\overline{\mathbf{G}}}_F(\mathbf{r}|\mathbf{r}') \cdot \mathbf{M}(\mathbf{r}')dS' \tag{11}$$
$$V_m(\mathbf{r}|\mathbf{r}') = \int_{S_0} G_{V_m}(\mathbf{r}|\mathbf{r}')q_m(\mathbf{r}')dS' \tag{12}$$

where $\overline{\overline{\mathbf{G}}}_\mathbf{A}$ and $\overline{\overline{\mathbf{G}}}_\mathbf{F}$ are the dyadic Green's functions of Sommerfeld's choice [8].

In the above expressions the electric (magnetic) charge density is related to the electric (magnetic) current density through the continuity equation for electric (magnetic) current.

2.2 Mixed Potential Integral Equations

The mixed potential integral equations can be obtained by enforcing the boundary conditions such that the total electric fields vanish on the electric conductors and that the magnetic field is continuous through the aperture. Allowing for some ohmic losses on the conductors by assuming that the surface impedance for the patch and feedline are both Z_s, the following three coupled MPIEs are obtained:

1) On the patch in region 1 $(z = h_1)$

$$\hat{z} \times \left(-j\omega \int\limits_{S_p} \overline{\overline{\mathbf{G}}}_A^{(1)} \cdot \mathbf{J}_p dS' - \nabla \int\limits_{S_p} G_v^{(1)} \rho_p dS' - Z_s \mathbf{J}_p \right.$$
$$\left. + (1/\epsilon_1) \int\limits_{S_{ap}} \mathbf{G}_{EM}^{xy(1)} \cdot \mathbf{M}_{ap} dS' \right) = 0 \quad (13)$$

2) On the feedline in region 2 $(z = -h_2)$

$$\hat{z} \times \left(-j\omega \int\limits_{S_p} \overline{\overline{\mathbf{G}}}_A^{(2)} \cdot \mathbf{J}_f dS' - \nabla \int\limits_{S_p} G_v^{(2)} \rho_f dS' - Z_s \mathbf{J}_f \right.$$
$$\left. - (1/\epsilon_2) \int\limits_{S_{ap}} \mathbf{G}_{EM}^{xy(2)} \cdot \mathbf{M}_{ap} dS' + E^e \right) = 0 \quad (14)$$

3) In the aperture $(z = 0)$

$$\hat{z} \times \left(+ j\omega \int\limits_{S_{ap}} \overline{\overline{\mathbf{G}}}_F^{(1)} \cdot \mathbf{M}_{ap} dS' - \nabla \int\limits_{S_{ap}} G_{V_m}^{(1)} \rho_{m_{ap}}^{(1)} dS' \right.$$
$$\left. - (1/\mu_0) \int\limits_{S_p} \mathbf{G}_{HJ}^{yx(1)} \mathbf{J}_f dS' \right)$$
$$= \hat{z} \times (-j\omega \int\limits_{S_{ap}} \overline{\overline{\mathbf{G}}}_F^{(2)} \cdot \mathbf{M}_{ap} dS' - \nabla \int\limits_{S_{ap}} G_{V_m}^{(2)} \rho_{m_{ap}}^{(2)} dS'$$
$$- (1/\mu_0) \nabla \times \int\limits_{S_f} \mathbf{G}_{HJ}^{yx(2)} \mathbf{J}_f dS') \quad (15)$$

and $G_{HJ}^{yx} = -G_{EM}^{xy}$. These are the Green's functions for the associated coupled fields in the region considered and can be expressed as

$$G_{HJ}^{xy} = \frac{1}{\mu_0}\left[\frac{\partial G_A^{xx}}{\partial z} - \frac{\partial G_A^{zx}}{\partial x}\right]_{z=0,\, z'=h} \tag{16}$$

If all the other boundary conditions are satisfied by the Green's functions, the problem is fully formulated by the above three mixed potential integral equations which can be solved for the various unknown surface currents.

2.3 Method of Moments

The moment method is applied to solve the integral equations (13)–(15) and the approach is similar to [4] where the rooftop basis function and razor test functions are used. In a similar manner, the patch, feedline and the aperture are divided into charge cells. Let there be M and N electric current cells on the patch x and y direction respectively, P electric current cells on the feedline (in the x-direction), and Q magnetic current cells on the aperture (in y-direction). The electric currents on the feedline and patch, and the magnetic currents on the aperture are expanded over a set of rooftop basis functions as

$$J_f = \hat{\mathbf{x}}\frac{1}{w_f}\sum_{j=1}^{P} I_{f\,xj} T_{fx}(\mathbf{r} - \mathbf{r}_{xj}) \tag{17}$$

$$J_p = \hat{\mathbf{x}}\frac{1}{w_p}\sum_{j=1}^{M} I_{p\,xj} T_{px}(\mathbf{r} - \mathbf{r}_{xj}) + \hat{\mathbf{y}}\frac{1}{l_p}\sum_{j=1}^{N} I_{pyj} T_{py}(\mathbf{r} - \mathbf{r}_{yj}) \tag{18}$$

$$M_{ap} = \hat{\mathbf{y}}\frac{1}{w_{ap}}\sum_{j=1}^{Q} K_{apyj} T_{ap\,y}(\mathbf{r} - \mathbf{r}_{yj}) \tag{19}$$

where $I_{f\,xj}$, $I_{pxj}(I_{pyj})$ and K_{apyj} are corresponding current coefficients; $\mathbf{r}_{xj}$ and $\mathbf{r}_{yj}$ are the vectors denoting the centre of the corresponding current cells.

The rooftop basis function $T_x(T_y)$ is given by:

$$T_s(r) = \begin{cases} 1 - |x|/l & |x| < l,\ |y| < \frac{w}{2} \\ 0 & \text{elsewhere} \end{cases} \tag{20}$$

where $s = x$ or y, and w is the width and l is the length of the charge cell considered.

By the continuity equations for electric and magnetic current densities, the associated electric and magnetic charge densities are obtained as follows:

$$q_f = \frac{1}{j\omega w_f l_f} \sum_{j=1}^{P} I_{f\,xj}[\Pi_f(\mathbf{r} - \mathbf{r}_{xj}^+) - \Pi_f(\mathbf{r} - \mathbf{r}_{xj}^-)] \tag{21}$$

$$q_p = \frac{1}{j\omega w_p l_p} \Bigg\{ \sum_{j=1}^{M} I_{p\,xj}[\Pi_p(\mathbf{r} - \mathbf{r}_{xj}^+) - \Pi_p(\mathbf{r} - \mathbf{r}_{xj}^-)] + \sum_{j=1}^{N} I_{pyj}[\Pi_p(\mathbf{r} - \mathbf{r}_{yj}^+) - \Pi_p(\mathbf{r} - \mathbf{r}_{yj}^-)] \Bigg\} \tag{22}$$

$$q_{map} = \frac{1}{j\omega w_{ap} l_{ap}} \sum_{j=1}^{Q} K_{apyj}[\Pi_{ap}(\mathbf{r} - \mathbf{r}_{yj}^+) - \Pi_{ap}(\mathbf{r} - \mathbf{r}_{yj}^-)] \tag{23}$$

where Π is a two dimensional unit pulse function and $\mathbf{r}_{xj}^+$, $\mathbf{r}_{xj}^-$, $\mathbf{r}_{yj}^+$ and $\mathbf{r}_{yj}^-$ are the vectors denoting the centre of the corresponding charge cells.

To simplify the notation, we introduce the discrete Green's functions relating to the potentials and fields based on the basis functions defined above. From [4], we have:

$$\Gamma_A^{xx}(\mathbf{r}|\mathbf{r}_{xj}) = \frac{1}{\mu_0 k_o} \int\limits_{S_{xj}} G_A^{xx}(\mathbf{r}|\mathbf{r}') T_x(\mathbf{r}|\mathbf{r}')(k_0^2 dS') \tag{24}$$

$$\Gamma_V(\mathbf{r}|\mathbf{r}_{xj}) = \frac{\epsilon_0}{k_0} \int\limits_{S_{0j}} G_V(\mathbf{r}|\mathbf{r}')\Pi(\mathbf{r}' - \mathbf{r}_{0j})(k_0^2 dS') \tag{25}$$

In addition, we define the discrete Green's functions electric vector potential and magnetic scalar potential as:

$$\Gamma_F^{yy}(\mathbf{r}|\mathbf{r}_{yj}) = \frac{1}{\epsilon k_0} \int\limits_{S_{apyj}} G_F^{yy}(\mathbf{r}|\mathbf{r}') T_y(\mathbf{r}' - \mathbf{r}_{yj})(k_0^2 dS') \tag{26}$$

$$\Gamma_{V_m}(\mathbf{r}|\mathbf{r}_{yj}) = \frac{\mu_0}{k_0} \int\limits_{S_{ap\;0j}} G_{V_{mq}}(\mathbf{r}|\mathbf{r}')\Pi(\mathbf{r}' - \mathbf{r}_{0j})(k_0^2 dS') \tag{27}$$

with $S_{apyj}(S_{ap0j})$ is the area of the aperture current (charge) cell.

For the coupled fields G_{HJ}^{yx} and G_{EM}^{xy} another two notations are introduced

$$\Gamma_{HJ}^{yx}(\mathbf{r}|\mathbf{r}_{yj}) = \int_{S_{xj}} G_{HJ}^{yx}(\mathbf{r}|\mathbf{r}')T_x(\mathbf{r}' - \mathbf{r}_{xj})dS' \tag{28}$$

$$\Gamma_{EM}^{xy}(\mathbf{r}|\mathbf{r}_{yj}) = \int_{S_{apyj}} G_{EM}^{xy}(\mathbf{r}|\mathbf{r}')T_y(\mathbf{r}' - \mathbf{r}_{yj})dS' \tag{29}$$

Given the above surface current and charge distributions (21)–(23), we obtain the resultant potentials as the superposition integrals of the corresponding Green's function. Substituting into coupling equations (13)–(15) and applying the razor test function on each current cell, we obtained the following matrix equations:

$$1) \qquad [Z_p^{(1)}][I_p^{(1)}] - [T_{ap}^{(1)}][K_{ap}] = 0 \tag{30}$$

$$2) \qquad [Z_f^{(2)}][I_f^{(2)}] + [T_{ap}^{(2)}][K_{ap}] - [V^{e(2)}] = 0 \tag{31}$$

$$3) \qquad [C_p^{(1)}][I_p^{(1)}] - [Y_{ap}^{(1)}][K_{ap}] = [C_f^{(2)}][I_f^{(2)}] + [Y_{ap}^{(2)}][K_{ap}] \tag{32}$$

The matrices and their elements are defined as follows:

a) $[Z_p^{(1)}]$ - the $(M+N)\times(M+N)$ impedance matrix of the patch.

$$\begin{aligned} z_{pij}^{xx(1)} =& \frac{jZ_0}{k_0^2 w_p l_p}\Big[\Gamma_V^{(1)}(r_{xi}^+|r_{xj}^+) - \Gamma_V^{(1)}(r_{xi}^+|r_{xj}^-) \\ & - \Gamma_V^{(1)}(r_{xi}^-|r_{xj}^+) + \Gamma_V^{(1)}(r_{xi}^-|r_{xj}^-)\Big] \\ & - \frac{jZ_0}{w_p}\int_{C_{p\xi}} \Gamma_A^{xx(1)}(r_{xi}|r_{xj})dx - Z_s\frac{l_p}{w_p}\sigma_{ij} \end{aligned} \tag{33a}$$

$$\begin{aligned} z_{pij}^{xy(1)} =& \frac{jZ_0}{k_0^2 w_p l_p}\Big[\Gamma_V^{(1)}(r_{xi}^+|r_{yj}^+) - \Gamma_V^{(1)}(r_{xi}^+|r_{yj}^-) \\ & - \Gamma_V^{(1)}(r_{xi}^-|r_{yj}^+) + \Gamma_V^{(1)}(r_{xi}^-|r_{yj}^-)\Big] \end{aligned} \tag{33b}$$

Similar expression is obtained for $z_{pij}^{yy(1)}$, and it is also noted that $z_{pij}^{xy(1)} = z_{pij}^{yx(1)}$.

b) $[Z_f^{(2)}]$ - the $P \times P$ impedance matrix of the feedline.

$$\begin{aligned} z_{fij}^{xx(2)} =& \frac{jZ_0}{k_0^2 w_f l_f}\Big[\Gamma_V^{(2)}(r_{xi}^+|r_{xj}^+) - \Gamma_V^{(2)}(r_{xi}^+|r_{xj}^-) \\ & - \Gamma_V^{(2)}(r_{xi}^-|r_{xj}^+) + \Gamma_V^{(2)}(r_{xi}^-|r_{xj}^-)\Big] \\ & - \frac{jZ_0}{w_f}\int\limits_{C_{fxi}} \Gamma_A^{xx(2)}(r_{xi}|r_{xj})dx - Z_s\frac{l_f}{w_f}\sigma_{ij} \end{aligned} \tag{34}$$

c) $[Y_{ap}^{(k)}]$ - the $Q \times Q$ admittance matrix of the aperture in region 1 or 2 ($k = 1$ or 2).

$$\begin{aligned} y_{apij}^{yy(k)} =& \frac{jY_0}{k_0^2 w_{ap} l_{ap}}\Big[\Gamma_{V_m}^{(k)}(r_{yi}^+|r_{yj}^+) - \Gamma_{V_m}^{(k)}(r_{yi}^+|r_{yj}^-) \\ & - \Gamma_{V_m}^{(k)}(r_{xi}^-|r_{xj}^+) + \Gamma_{V_m}^{(k)}(r_{xi}^-|r_{xj}^-)\Big] \\ & - \frac{jY_0}{w_{ap}}\int\limits_{C_{apyi}} \Gamma_F^{yy(k)}(r_{yi}|r_{yj})dy \end{aligned} \tag{35}$$

d) $[C_p^{(1)}]$ - the $Q \times (M+N)$ transfer matrix of the patch.

$$c_{pij}^{(1)} = \frac{1}{w_p}\int\limits_{C_{apyi}} \Gamma_{HJ}^{yx(1)}(r_{yi}|r_{xj})dy \tag{36}$$

e) $[C_f^{(2)}]$ - the $Q \times P$ transfer matrix of the feedline.

$$c_{fij}^{(2)} = \frac{1}{w_f}\int\limits_{C_{apyi}} \Gamma_{HJ}^{yx(2)}(r_{yi}|r_{xj})dy \tag{37}$$

f) $[T_{ap}^{(1)}]$ - the $P \times Q$ transfer matrix of the aperture in region 1.

$$t_{apij}^{(1)} = \frac{1}{w_{ap}}\int\limits_{C_{fxi}} \Gamma_{EM}^{xy(1)}(r_{xy}|r_{yj})dx \tag{38}$$

g) $[T_{ap}^{(2)}]$ - the $(M+N) \times Q$ transfer matrix of the aperture in region 2.

$$t_{apij}^{(2)} = \frac{1}{w_{ap}} \int\limits_{C_{pxi}} \Gamma_{EM}^{xy(1)}(r_{xy}|r_{yj})dx \tag{39}$$

where C_{fxi}, $C_{pxi}(C_{pyi})$, and C_{apyi} are the test segments of the corresponding current cells.

The excitation model of [4] can be similarly applied by placing the excitation current distribution over the charge cell located at the end of the feedline. We obtain the excitation vector $[V_e^{(1)}]$ as

$$v_{xi}^{e} = \frac{jZ_0}{k_0^2 ab}[\Gamma_V(r_{xi}^{+}|r_e) - \Gamma_V(r_{xi}^{-}|r_e)] \qquad (i = 1 \ldots P) \tag{40}$$

Solving the matrix equations yields the unknown current vector as:

$$[K_{ap}] = \frac{[C_f^{(2)}][Z_f^{(2)}]^{-1}[V_e^{(2)}]}{[Y_{ap}^{(1)}] + [Y_{ap}^{(2)}] - [C_p^{(1)}][Z_p^{(1)}][T_{ap}^{(1)}] - [C_f^{(2)}][Z_f^{(2)}][T_{ap}^{(2)}]} \tag{41}$$

$$[I_p^{(1)}] = [Z_p^{(1)}]^{-1}[T_{ap}^{(1)}][K_{ap}] \tag{42}$$

$$[I_f^{(2)}] = -[Z_f^{(2)}]^{-1}\left\{[T_{ap}^{(2)}][K_{ap}] - [V_e^{(2)}]\right\} \tag{43}$$

where $[K_{ap}] = [K_{ap}^{(1)}] = [K_{ap}^{(2)}]$.

The numerical calculation involved in solving for these current vectors is still a formidable task. In order to increase the computation speed, approximations for the surface and line integrals (as in [4]) can be applied to the above matrix elements when the source and field distance is sufficiently large. Since the coupling effect is dominated by the coupled fields in the vicinity of the aperture, the associated matrix elements of the coupling matrices with large source and field can effectively be neglected.

3. RESULTS

3.1 Results for Green's Functions

To confirm the valid use of the closed-form Green's functions in our algorithm, the accuracy of the relevant Green's functions in (13)–(15) are tested. Before the moment method is applied, the computed results

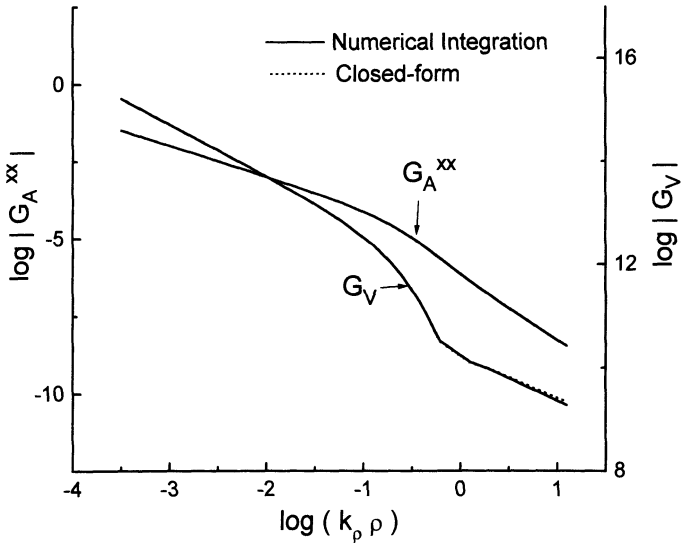

Figure 2. Magnitude of magnetic vector potential and electric scalar potential vs. radial distance from field to source (Operating frequency: 5 GHz). Substrate parameters: $h = 1.524$ mm, $\epsilon_r = 2.54$.

for the Green's functions evaluated by straight numerical integration of the Sommerfeld integral and the closed-form Green's functions are compared. For G_A^{xx} and G_V, where the source and field positions are both on the dielectric surface, the closed-form expressions are given in [5]. Numerical results are shown in Fig. 2 for a given substrate.

For G_F^{yy} and G_{V_m}, where the source and field positions are both on the aperture, closed-form expressions can be obtained using the procedure of [6] in which the Green's functions in the spectral domain are expressed in terms of transmission coefficients and the incident and reflected fields. Numerical results are shown in Fig. 3.

To obtain the closed-form approximation for $G_{HJ}^{yx}(G_{EM}^{yx})$, we treat the two differential terms of (16) separately. By differentiating with respect to z all the field components of G_A^{xx} in the spatial domain, a closed-form for $\partial G_A^{xx}/\partial z$ can be obtained. On the other hand, G_A^{zx} can not be expressed in terms of incident and reflected fields and thus the extraction of the various field components is not possible. Fortunately, the curve of G_A^{zx} decays rapidly in the spectral domain which allows us to make an exponential approximation of the integrand for

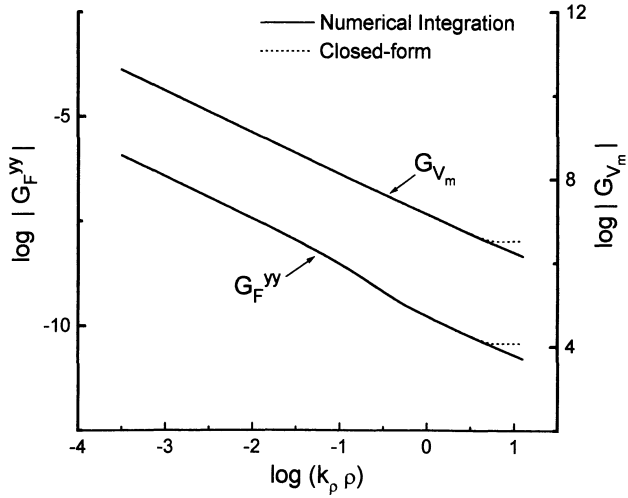

Figure 3. Magnitude of electric vector potential and magnetic scalar potential vs. radial distance from field to source (Operating frequency: 5 GHz). Substrate parameters: $h = 1.524$ mm, $\epsilon_r = 2.54$.

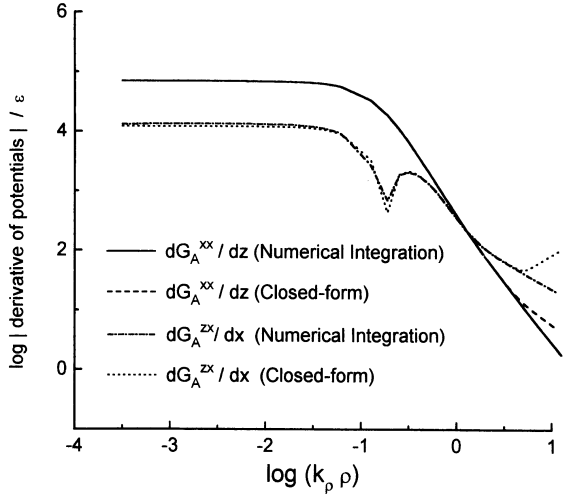

Figure 4. Magnitude of Green's functions relating to the coupled fields vs. radial distance from field to source (Operating frequency: 5 GHz). Substrate parameters: $h = 1.524$ mm, $\epsilon_r = 2.54$.

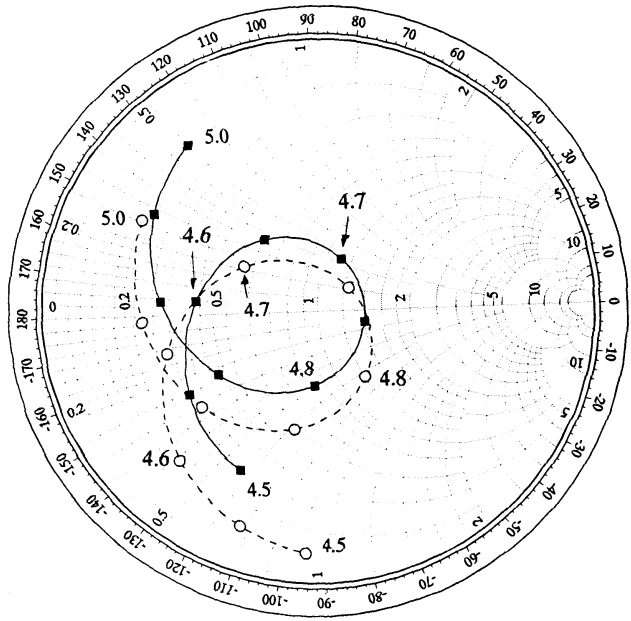

Figure 5. Smith chart plot of input impedance of the aperture coupled patch antenna. Antenna parameters: $\epsilon_{rl} = 2.54$, $h_1 = 1.524$ mm, $L_p = 18$ mm, $W_p = 15$ mm, $x_{os} = 0$ mm, $y_{os} = 0$ mm, $L_{ap} = 9$ mm, $W_{ap} = 0.5$ mm, $\epsilon_{rl} = 2.54$, $h_1 = 1.524$ mm, $L_f = 55$ mm, $W_f = 1.2$ mm, $L_s = 10$ mm, $(\tan\delta_1 = \tan\delta_2 = 0.001)$. No. of cells on feedline = 55. Frequency range: 4.5 GHz–5.0 GHz (0.5 GHz step). —□— Measured - - ○ - - Calculated

G_A^{zx} with reasonable accuracy and a closed-form approximation can similarly be obtained for $\partial G_A^{zx}/\partial dx$. Fig. 4 shows the numerical results for these two Green's functions. It is observed that the closed-form results for $\partial G_A^{zx}/\partial dx$ is less accurate than the other Green's functions. However, this has only negligible effect on the accuracy of our overall results because the coupled field is more dominated by the term $\partial G_A^{xx}/\partial z$.

From these curved, we notice that accuracy of the closed-form Green's functions begin to break down as the distance between source and field points exceeds certain limits; this was pointed out in [7]. However, this error has only insignificant effects on our overall result

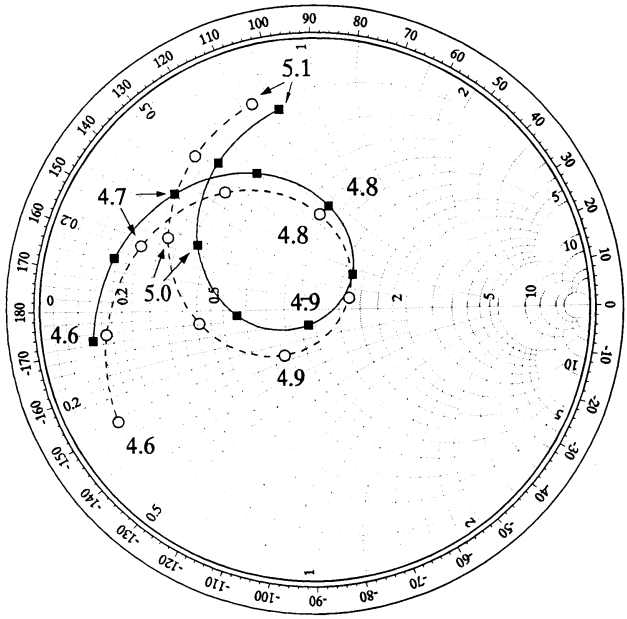

Figure 6. Smith chart plot of input impedance of the aperture coupled patch antenna. Antenna parameters: $\epsilon_{rl} = 2.54$, $h_1 = 1.524$ mm, $L_p = 18$ mm, $W_p = 15$ mm, $x_{os} = 0$ mm, $y_{os} = 0$ mm, $L_{ap} = 8$ mm, $W_{ap} = 0.5$ mm, $\epsilon_{rl} = 2.17$, $h_1 = 0.787$ mm, $L_f = 55$ mm, $W_f = 1.2$ mm, $L_s = 10$ mm, $(\tan\delta_1 = \tan\delta_2 = 0.001)$. No. of cells on feedline = 58. Frequency range: 4.6 GHz–5.1 GHz (0.5 GHz step). —□— Measured - - ○ - - Calculated

because in reality the size of antenna structure is such that the source-field distance always lies within the range of accurate approximations.

3.2 Results for Input Impedance

In our analysis the reference plane is at the center of the excitation cell which is located at the end of the feedline, so that it is not appropriate to compare our theoretical results with those of [2, 3] which assume the feedline is of infinite length. Two antennas with operating frequency of about 5 GHz were tested. Measurements were taken by a HP8510C network analyser. In these tests the numbers of charge cells on the patch in x and y directions are 9 an 7 respectively with 5 charge

cells on the aperture. Fig. 5 and Fig. 6 show on the Smith chart plots of the two antennas. The antenna's substrates for the radiating patch and feeding network are the same in the first case, and different in the second. It can be seen that the calculations agree very well with measurements with only a slight shifts in the prediction resonant frequency. Numerical convergence test on our algorithm has shown that the rate of convergence of resonant frequency against the number of basis functions in x-direction is relatively slow, and the predicted resonant frequency converges to the measured value as more cells are added along the resonant length of the patch. The discrepancy could also be due to error introduced to the measurement by the small air-gaps between the two layers of dielectric.

The calculated results of these plots were computed by the IBM Pentium 100 MHz PC. The run time required in the computation of input impedance for each frequency is approximately 30 seconds. Further increase in speed can be achieved if the approximation of the matrix elements discussed in previous section is utilised to a greater extent.

4. CONCLUSION

The validity of the proposed model using MPIE has been confirmed by showing the good agreement between theory and experiment. Most important is the sole use of closed-form Green's function in our analysis that enable us to compute the result with considerably less numerical effort in much higher speed than the spectral domain approach.

REFERENCES

1. Pozar, D. M., "Microstrip antenna aperture-coupled to a microstripline," *Electron. Lett.,* Vol. 21, No. 2, 49–50, January 1985.
2. Sullivan, P. L., and D. H. Schaubert, "Analysis of an aperture coupled microstrip antenna," *IEEE Trans. Antennas Propagation,* Vol. 34, 977–984, August 1986.
3. Pozar, D. M., "A reciprocity method of analysis for printed slot and slot-coupled microstrip antennas," *IEEE Trans. Antennas Propagation,* Vol. 34, 1439–1446, December 1986.
4. Mosig, J. R., and F. E. Gardiol, "General integral equation formation for microstrip antennas and scatterers," *IEE Procs.,* Vol. 132H, 424–432, 1985.

5. Chow, Y. L., J. J. Yang, and G. E. Howard, "Closed-form spatial Green's function for the thick substrate," *IEEE Trans. Microwave Theory Tech.,* Vol. 39, 588–592, March 1991.
6. Fang, D. G., J. J. Yang, and G. Y. Delisle, "Discrete image theory for horizontal electric dipoles in a multilayered medium," *IEE Proc.,* Vol. 135H, 297–303, 1988.
7. Aksun, M. I., and R. Mittra, "Derivation of closed-form Green's function for a general microstrip geometry," *IEEE Trans. Antennas Propagation.,* Vol. 40, 2055–2061, November 1992.
8. Sommerfeld, A., *Partial Differential Equations in Physics,* Academic Press, New York, 1949.